Mouse cytomegalovirus M36 and M45 death suppressors cooperate to prevent inflammation resulting from antiviral programmed cell death pathways

Lisa P. Daley-Bauer[a,1], Linda Roback[a], Lynsey N. Crosby[a], A. Louise McCormick[a], Yanjun Feng[a], William J. Kaiser[a], and Edward S. Mocarski[a,1]

[a]Department of Microbiology and Immunology, Emory Vaccine Center, Emory University School of Medicine, Atlanta, GA 30322

Edited by Michael B. A. Oldstone, The Scripps Research Institute, La Jolla, CA, and approved February 17, 2017 (received for review October 10, 2016)

The complex interplay between caspase-8 and receptor-interacting protein (RIP) kinase RIP 3 (RIPK3) driving extrinsic apoptosis and necroptosis is not fully understood. Murine cytomegalovirus triggers both apoptosis and necroptosis in infected cells; however, encoded inhibitors of caspase-8 activity (M36) and RIP3 signaling (M45) suppress these antiviral responses. Here, we report that this virus activates caspase-8 in macrophages to trigger apoptosis that gives rise to secondary necroptosis. Infection with double-mutant ΔM36/M45mutRHIM virus reveals a signaling pattern in which caspase-8 activates caspase-3 to drive apoptosis with subsequent RIP3-dependent activation of mixed lineage kinase domain-like (MLKL) leading to necroptosis. This combined cell death signaling is highly inflammatory, greater than either apoptosis induced by ΔM36 or necroptosis induced by M45mutRHIM virus. IL-6 production by macrophages is dramatically increased during double-mutant virus infection and correlates with faster antiviral responses in the host. Collaboratively, M36 and M45 target caspase-8 and RIP3 pathways together to suppress this proinflammatory cell death. This study reveals the effect of antiviral programmed cell death pathways on inflammation, shows that caspase-8 activation may go hand-in-hand with necroptosis in macrophages, and revises current understanding of independent and collaborative functions of M36 and M45 in blocking apoptotic and necroptotic cell death responses.

MCMV | caspase-8 | RIP3 kinase | cell death | inflammation

Regulated cell death is an important host response to injury, inflammation, and infection. Two interlinked outcomes of regulated cell death play out naturally in host defense against invading intracellular pathogens: alternate caspase-8–mediated apoptosis and receptor-interacting protein (RIP) kinase RIP 3 (RIPK3)-mediated programmed necrosis (necroptosis) (1). Morphologically, apoptosis has been defined by cell shrinkage, chromatin condensation, and membrane blebbing, whereas necrosis is marked by cell swelling, disruption of the plasma membrane, and the release of intracellular contents. Necroptosis, a pathway believed to be unleashed when caspase-8 is blocked, is dependent on RIP homotypic interaction motif (RHIM) signaling via RIP3 and consequent activation of mixed lineage kinase-like (MLKL), leading to the disruption of cellular membranes. Evidence suggests that caspase-8–mediated apoptosis may be triggered by RIP3 when overexpressed (2), mutations are introduced (3), small molecule kinase inhibitors are used (4), or in response to influenza A virus (5). The importance of these alternate forms of cell death was first recognized in mice infected with murine cytomegalovirus (MCMV) (6–8), as well as through the dysregulation associated with germ-line elimination of caspase-8 (9-11). Mechanisms, however, were unveiled in cell-based studies and have best been characterized in TNFR1 death receptor signaling executed through cytosolic complexes nucleated by RIP1 (12-14). Although the importance of caspase-8, RIP1, and RIP3 emerged from studies of death receptor signaling, a similar complex, termed a Ripoptosome, that incorporates Fas-associated protein with death domain (FADD) and cellular FLICE-inhibitory protein (cFLIP) forms downstream of pathogen-sensors (4), whether triggered by RIP1, the Toll-like receptor (TLR)3/TLR4 adaptor protein TRIF (15), or the viral sensor DNA-dependent activator of IFN (DAI) (8). As a consequence, cell autonomous death pathways provide host defense against obligate intracellular pathogens, including bacteria and viruses (16).

Both apoptosis (5, 17, 18) and necroptosis (7, 8, 12) have the potential to limit viral infection. The most compelling evidence supporting the contribution of cell death to antiviral immunity is the growing number of pathogen-encoded cell death suppressors that have been identified (19). MCMV, a natural β-herpesvirus of mice, encodes a viral inhibitor of caspase activation (M36), as well as a viral inhibitor of RIP activation (M45). Similar to the human (H)CMV homolog encoded by UL36 (17), M36-encoded viral inhibitor of caspase activation blocks both basal and activated caspase-8 protease activity. M45-encoded viral inhibitor of RIP activation is a RHIM signaling suppressor (6, 20) that prevents the activation of RIP3 and subsequent activation of MLKL (8, 15). M45 contributes to activation as well as suppression of NF-κB levels in infected cells (21), but is more physiologically important as a cell death suppressor preventing necroptosis during infection of the natural host animal (7, 8). M36 and M45 mutants have validated the significance of caspase-8 and RIP3 cell death signaling in limiting replication in the host over any effect on NF-κB.

Significance

Caspase-8–mediated apoptotic and receptor-interacting protein (RIP)-dependent necroptotic signaling pathways are recognized host defense mechanisms that act by eliminating virus-infected cells. Cytomegalovirus-encoded inhibitors of apoptosis and necroptosis sustain infection and pathogenesis by preventing specific programmed cell death pathways. In the absence of viral inhibitors, combined apoptotic–necroptotic cell death signaling halts infection, preventing the virus from gaining a foothold in the host. We describe natural cooperation between apoptosis and necroptosis pathways in macrophages and within the host, resulting in robust proinflammatory cytokine responses not observed when infected cells die by either apoptosis or necroptosis alone. Thus, apoptosis combined with necroptosis serves a dual role in limiting herpesvirus persistence in the host.

Author contributions: L.P.D.-B., W.J.K., and E.S.M. designed research; L.P.D.-B., L.R., and Y.F. performed research; L.P.D.-B., L.N.C., A.L.M., and W.J.K. contributed new reagents/analytic tools; L.P.D.-B. analyzed data; and L.P.D.-B. and E.S.M. wrote the paper.

The authors declare no conflict of interest.

This article is a PNAS Direct Submission.

[1]To whom correspondence may be addressed. Email: ldaley@emory.edu or mocarski@emory.edu.

This article contains supporting information online at www.pnas.org/lookup/suppl/doi:10.1073/pnas.1616829114/-/DCSupplemental.

Infection of macrophages in culture with M36-deficient MCMV drives TNF-dependent, extrinsic apoptosis (22), and infection of cells with M45-deficient MCMV drives DAI initiation of RIP3-mediated necroptosis that cuts short infection in many cell types (7, 8). Death pathways are held in check by M36 (23, 24) and M45 (7), respectively, and viruses lacking these suppressors are significantly attenuated in the natural host (7, 23–25). Execution of MCMV M36 function sensitizes cells to necroptosis (9), but the natural role of caspase-8 inhibition in unleashing this pathway has only recently been revealed in studies with HSV-1 and HSV-2 in human cells (26). It remains to be determined whether caspase-8 suppression is important for unleashing MCMV-induced necroptosis in mice (19).

Given the documented antiviral effect of caspase-8–mediated apoptosis and DAI/RIP3 necroptosis on MCMV infection (27), we set out to investigate infection with ΔM36/M45mutRHIM double-mutant virus to interrogate the potential interplay between caspase-8 and RIP3 signaling pathways in host defense. We report the surprising finding that macrophages infected with double-mutant virus actually succumb to apoptotic death that progresses into secondary necroptosis, even though caspase-8 is fully activated. Importantly, this cell death signaling enhances IL-6 cytokine production in infected macrophage cultures and elicits faster inflammatory cytokine and CD8 T-cell responses in the host than those observed in any other infection setting. Thus, a picture emerges in which RIP3-pMLKL–driven necroptosis is unleashed downstream of caspase-8 activation during viral infection, setting in motion a highly proinflammatory cell death signaling cascade that facilitates host control over viral persistence.

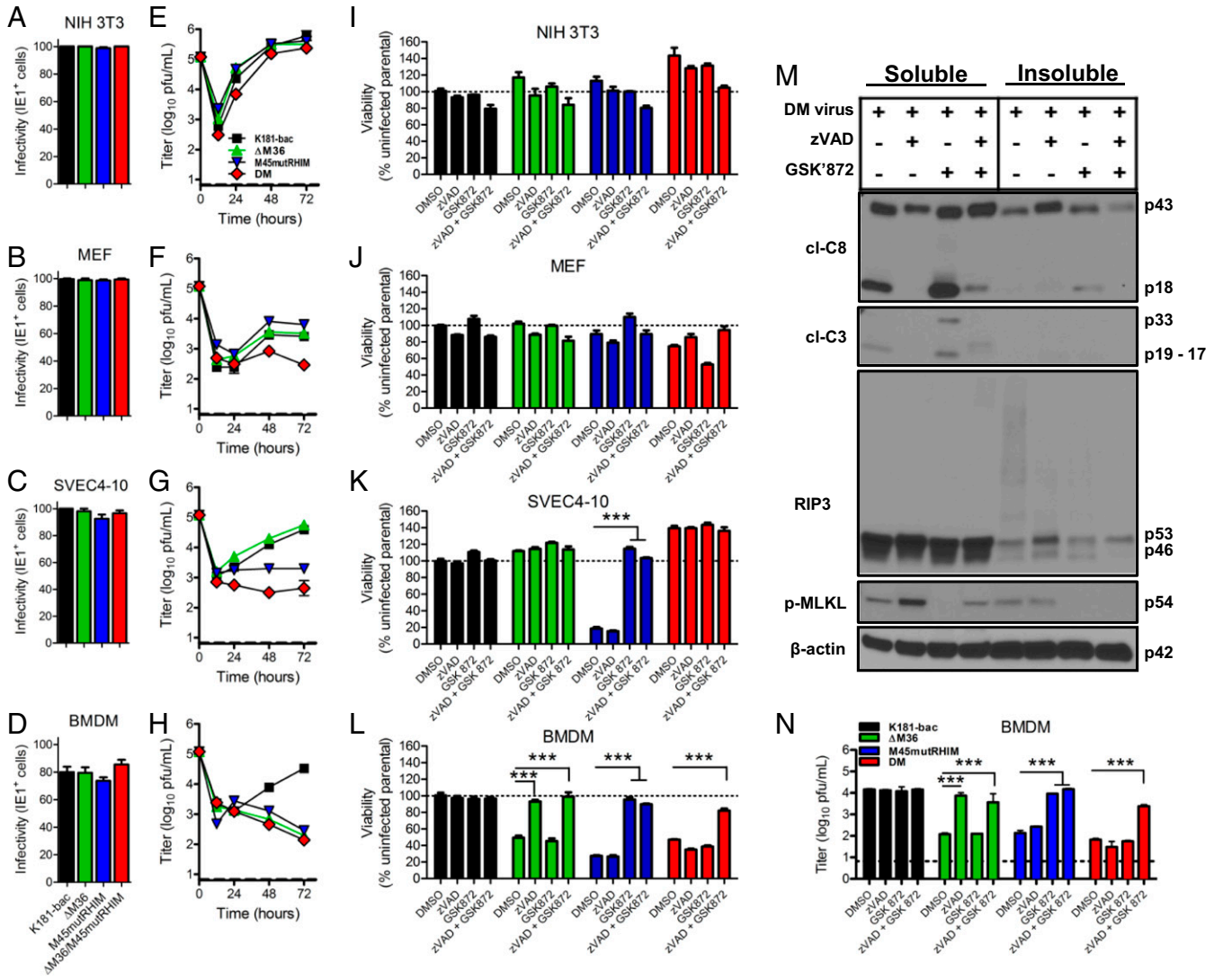

Fig. 1. MCMV triggers independent and dual caspase-8 and RIP3 cell death that is suppressed by M36 and M45 functions. (*A–D*) Infectivity of WT and mutant viruses in NIH 3T3, MEFs, SVEC4-10 cells, and BMDM, depicted as frequencies of IE1$^+$ cells. Cells were infected with a MOI of 5 or 10 (BMDM only) with any of the four viruses and assessed at 6 hpi for IE1 expression by immunofluorescence assay. (*E–H*) Replication levels of the four viruses in cells through 3 dpi (MOI = 5). Viral titers were determined by plaque assay at specified points. Horizontal dashed lines indicate the limit of detection of the assay. (*I–L*) Viability of infected cells [MOI = 5 or 10 (BMDM)] either untreated (DMSO; 0.1%) or treated with the pan-caspase inhibitor zVAD and/or the RIP3 inhibitor GSK872. Cell viability as measured by intracellular ATP levels, using the Cell Titer-Glo Luminescent Cell Viability Assay kit. Horizontal dotted lines indicate 100% viability. (*M*) Western blots showing RIP3, p-MLKL, cl-caspase-8 (cl-C8), and cl-caspase-3 (cl-C3) levels in BMDMs. Double-mutant virus-infected cells (MOI = 10) either untreated or treated with zVAD-fmk (zVAD, 25 μM), with or without GSK'872 (3 μM) for 9 (zVAD only) or 12 h. (*N*) Replication of viruses in BMDMs treated with caspase-8 and RIP3 inhibitory drugs. Double-mutant virus-infected cells (MOI = 5) were cultured with DMSO or drugs for 72 hpi. Panels represent at least two independent experiments. Error bars indicate SD of the mean. $P < 0.001$. DM, double-mutant.

Results

Double-Mutant MCMV Triggers Dual Caspase-8– and RIP3-Dependent Death in Infected Cells. To determine whether MCMV-induced necroptosis depends on caspase-8 inhibition by M36 and to unveil interdependencies between caspase-8– and RIP3-dependent host defense pathways, we used individual and combined M36 and M45 mutant viruses generated from a common parent virus (Fig. S1). K181 bacterial artificial chromosome (K181-bac) parental strain (M36 and M45 proficient), ΔM36 (proapoptotic), and M45mutRHIM (pronecroptotic) single mutants and ΔM36/M45mutRHIM double-mutant MCMV were used. Four different cell types were evaluated using conditions to achieve infection of all cells within a culture: multiplicity of infection (MOI) is 5 for NIH 3T3 and mouse embryonic fibroblasts (MEFs) and SVEC4-10 endothelial cells, and MOI is 10 for bone marrow-derived macrophages (BMDMs) (Fig. 1). According to immediate early (IE) protein detection (Fig. 1 *A–D*), these cell types were equally susceptible to K181-bac or mutant virus entry and initial gene expression after infection.

Single mutants demonstrated the expected pattern of compromise (24, 25) in replication (Fig. 1 *E–H*) and cell viability at 18 h postinfection (hpi; Fig. 1 *I–L*, DMSO bars). Double-mutant virus replicated efficiently in NIH 3T3 cells, but inefficiently or not at all in MEFs, SVEC4-10 cells, and BMDMs (Fig. 1 *E–H*). Compromised double-mutant virus replication correlated with the induction of cell death only in MEFs and BMDMs (Fig. 1 *I–L*). In endothelial cells, double-mutant virus replication was compromised even though cells remained viable (Fig. 1 *G* and *K*). MEFs were resistant to MCMV, although they supported replication of single-mutant viruses better than double-mutant virus (Fig. 1*F*). Poor growth of double-mutant virus was likely a result of induction of cell death evident at 18 hpi (Fig. 1*J*). SVEC4-10 cells supported K181-bac and ΔM36 viruses, but failed to support M45mutRHIM virus replication (Fig. 1*G*) because of previously identified (7, 8) DAI/RIP3-dependent necroptosis (Fig. 1*K*). The absence of cell death in double-mutant virus-infected SVEC4-10 cells is consistent with the contribution of M36-mediated suppression of caspase-8 in sensitizing cells to necroptosis (9). SVEC4-10 cells are insensitive to virus-induced apoptosis such that cell death is not triggered by ΔM36 MCMV (24). Finally, BMDMs failed to support replication of any mutant virus due to cell death induced by either caspases, RIP3, or both together (Fig. 1 *H* and *L*). Overall, these patterns implicate caspase-8 and RIP3 signaling pathways in cutting short viral replication during double-mutant virus infection by cell death-dependent and cell death-independent outcomes.

To better understand the signaling pathways that contribute to patterns of cell death and investigate how caspase-8 inhibition affects necroptosis, we used the pan-caspase inhibitor zVAD-fmk (zVAD) and RIP3 kinase inhibitor GSK'872 [from GlaxoSmithKline (GSK)] either alone or in combination to assess levels of cell death at 18 hpi (Fig. 1 *I–L*). All cell types remained viable during infection with K181-bac MCMV and after treatment with zVAD, GSK'872, or zVAD plus GSK'872. NIH 3T3 fibroblasts remained viable during infection, whether treated with small molecule inhibitors or not (Fig. 1*I*). In MEFs, double-mutant virus-induced death was modestly reversed by zVAD treatment, whereas GSK'872 alone sensitized to RIP3-mediated apoptosis in the expected pattern (4), where death was reversed by zVAD plus GSK'872 treatment (Fig. 1*J*). These data indicate that MEFs are sensitive to caspase-8–dependent death after double-mutant virus infection. In SVEC4-10 cells, M45mutRHIM virus-induced death was reversed by treatment with GSK'872 (Fig. 1*K*), as expected (4, 15). Surprisingly, zVAD addition did not compromise the viability of double-mutant virus-infected cells, suggesting zVAD was unable to substitute for virus-encoded M36 blockade of caspase-8 to trigger DAI/RIP3 necroptosis in infected cells. Here, we demonstrate that DAI/RIP3-dependent necroptosis is held in check by caspase-8 function in this cell type. SVEC4-10 cells represent one example where caspase-8 suppression appears to cut short replication by sensitizing to necroptosis, even though this cannot be replaced by zVAD. The reason why double-mutant virus nevertheless fails to replicate in SVEC4-10 cells remains to be investigated.

BMDMs represent an important cell type in MCMV infection, given the importance of patrolling monocyte-derived cells in the dissemination of MCMV (27–29), and this being the cell type in which CMV-encoded cell death suppressors that block apoptotic pathways are physiologically relevant. BMDMs exhibited sensitivity to death induced by ΔM36, M45mutRHIM, and double-mutant viruses (Fig. 1*L*) in a pattern reflecting the effect on viral replication (Fig. 1*H*). Here, zVAD was sufficient to reverse caspase-8–dependent death from ΔM36 virus and GSK'872 was sufficient to prevent RIP3-dependent death from M45mutRHIM virus. Importantly, combined zVAD plus GSK'872 treatment prevented death from double-mutant virus. These data suggest a combined apoptotic and necroptotic death pattern when both virus-encoded suppressors are absent, raising a question regarding the interplay of apoptotic and necroptotic cell death pathways within infected BMDMs.

M36 and M45 Cooperate to Suppress Dual Caspase-8– and RIP3-Dependent Death. We next conducted immunoblot analyses on double-mutant virus-infected cells to better understand the effect of inhibiting caspase-8 and RIP3 signaling pathways on cell death using zVAD and GSK'872, respectively. Levels and distribution of cell death signaling components in soluble and insoluble cell lysate fractions (12, 14, 30) were evaluated (Fig. 1*M*). Infection resulted in detection of cleaved (cl-) caspase-8 and caspase-3, as well as phospho (p)-MLKL in the soluble fraction at 12 hpi. At this time, cl-caspase-8 p43, RIP-3, and p-MLKL were also detected in the insoluble fraction, where slower-migrating forms of RIP3 may reflect proposed ubiquitin modification (31). zVAD inhibited the accumulation of p18, but not p43, forms of cl-caspase-8; blocked caspase-3 cleavage; reduced RIP3 p46 levels; and intensified p-MLKL levels in the soluble fraction, consistent with enhanced necroptosis, while reducing RIP3 modification in the insoluble fraction. Cl-caspase-8 and cl-caspase-3 levels increased in the presence of RIP3 kinase inhibitor GSK'872, indicating enhanced apoptosis compared with untreated double-mutant-infected cells. Combined zVAD and GSK'872 treatment reduced caspase-8 and caspase-3 cleavage in the soluble fraction, and RIP3 processing and partitioning of p-MLKL into the insoluble fraction. Together, these data reveal that BMDMs engage both apoptotic and necroptotic machinery during double-mutant virus infection, triggering alternate apoptosis and necroptosis, depending on whether caspase-8 or RIP3 kinase activity is suppressed. Thus, M36 and M45 must cooperate to suppress dual caspase-8– and RIP3-dependent death.

We next used zVAD and GSK'872 to understand the effect of caspase-8 and RIP3 signaling on viral replication in BMDMs at 72 hpi from treated (Fig. 1*N*). Conditions that sustained cell survival (Fig. 1*L*) normalized mutant virus replication such that titers were similar to parental K181-bac virus (Fig. 1*N*). zVAD inhibition of caspase activity increased ΔM36 virus levels at 72 hpi >60-fold. GSK'872 inhibition of RIP3 kinase activity increased M45mutRHIM virus titers ~80-fold. zVAD and GSK'872 together increased double-mutant virus levels 40-fold (Fig. 1 *L* and *N*), although individually, neither zVAD nor GSK'872 had any effect. Thus, caspase-8 and RIP3 signaling pathways undermine viral replication unless suppressed by M36 and M45, respectively. These data indicate that combined inhibitors of apoptotic and necroptotic death are able to rescue double-mutant virus replication in BMDMs, but blockade of either death pathway triggers the alternate pathway.

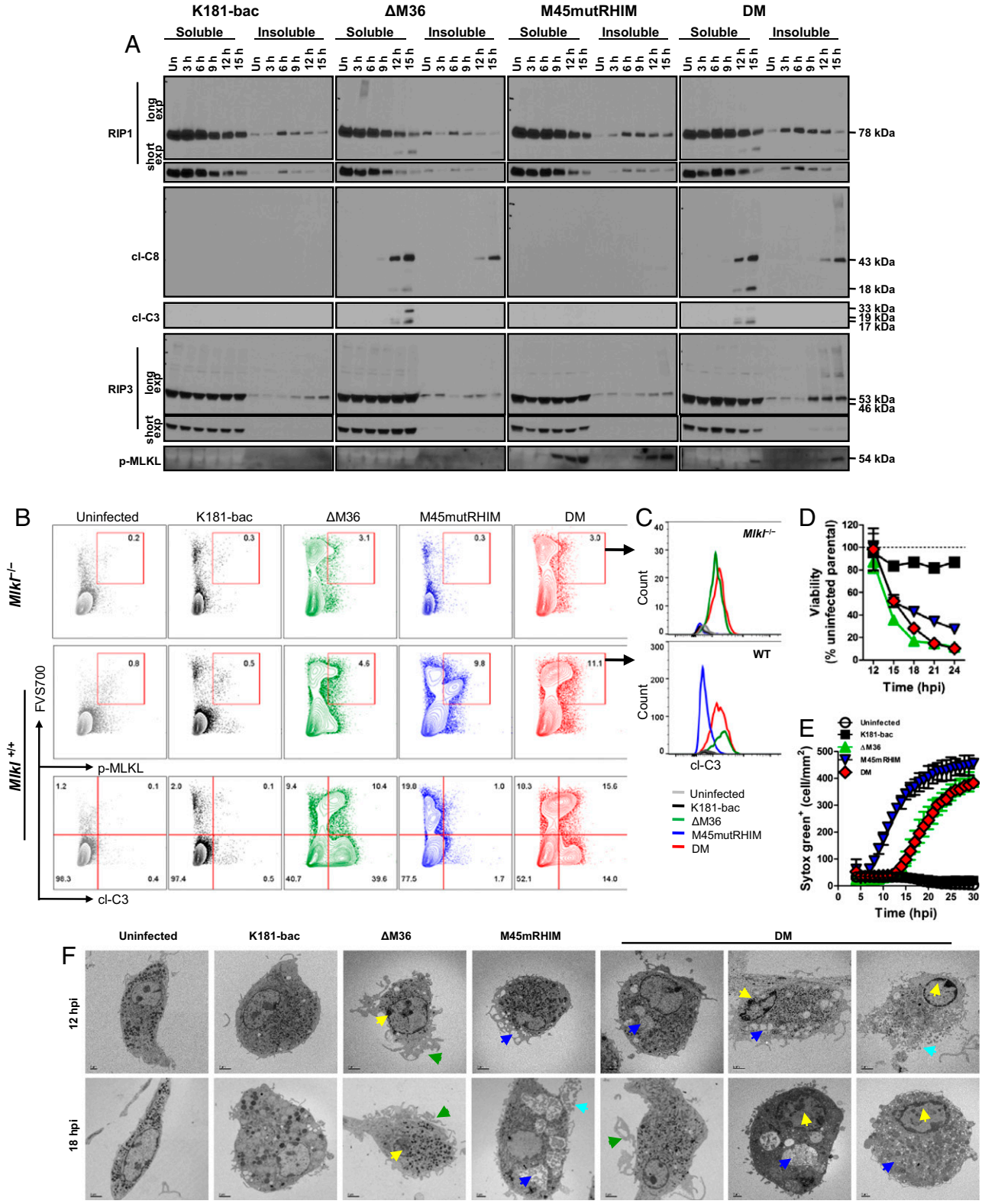

Fig. 2. Double-mutant virus infection induces caspase-8–mediated apoptosis with delayed RIP3-dependent necroptosis. (*A*) Western blots showing RIP1, RIP3, cl-C8, cl-C3, and p-MLKL levels in BMDM. Cells were either uninfected or infected (MOI = 10) with K181-bac, ΔM36, M45mutRHIM, or double-mutant virus for the specified times. (*B* and *C*) Flow cytometry plots of virus-infected *Mlkl*$^{-/-}$ and *Mlkl*$^{+/+}$ BMDMs at 15 hpi showing (*B*) FVS700 with p-MLKL or cl-C3 expression or (*C*) cl-C3 expression by FVS700^{+} p-MLKL^{+} cells. (*D*) Change in BMDM viability over time after infection. Horizontal dotted line indicates 100% viability. (*E*) SYTOX Green accumulation over time in permeable, necrotic BMDMs after infection. (*F*) Transmission electron microscopy images of BMDMs either uninfected or infected 12 and 18 hpi with specified virus (MOI = 10). Apoptosis markers: yellow arrows, condensed chromatin; green arrows, ruffling/blebbing. Necroptosis markers: dark blue arrows, vacuoles; light blue arrows, lysis.

Double-Mutant Virus Triggers Apoptosis Before Necroptosis in BMDMs. Given the sensitivity to caspase-8 and/or RIP3-driven death, BMDMs were used to define cell death signaling mechanisms. Immunoblot analyses at 3-h intervals through 15 hpi tracked levels and distribution of cell death signaling components (Fig. 2*A*). RIP1 and RIP3 kinases partitioned predominantly to the soluble fraction in uninfected BMDMs without evidence of cl-caspase-8, caspase-3, or p-MLKL in either fraction (Fig. 2*A*, lanes 1). In K181-bac virus-infected cells in which M36 and M45 functions were intact, soluble RIP1 levels decreased after 6 hpi, when insoluble RIP1 levels peaked, whereas soluble RIP3 levels persisted through 15 hpi and insoluble RIP3 increased by 9 hpi without expressing any markers of active cell death (Fig. 2*A*; K181-bac). ΔM36 virus-infected cells differed from K181-bac virus infection in that soluble cl-caspase-8 and caspase-3 were detected by 9 and 12 hpi, respectively, with cl-caspase-8 detected in the insoluble fraction by 12 hpi (Fig. 2*A*; ΔM36). In addition, modified soluble RIP1 appeared by 3 hpi, before caspase cleavage was detected, whereas soluble and insoluble cleaved RIP1 were detected at 12 and 15 hpi, respectively. In contrast, M45mutRHIM virus-infected cells showed p-MLKL in soluble and insoluble fractions by 9 hpi, consistent with induction of the expected death pathway (Fig. 2*A*; M45mutRHIM). Finally, double-mutant virus triggered a pattern of cell death markers consistent with apoptosis in the absence of M36 function, as well as necroptosis in the absence of M45 function, even though the kinetics of necroptosis were delayed (Fig. 2*A*; double-mutant). Cleavage of soluble caspases and RIP1 proceeded without evidence of modified RIP1 at 3 hpi, but was accompanied by more abundant insoluble RIP1 starting at 3 hpi, as well as modified forms of insoluble RIP3 starting at 9 hpi. Slowly migrating species of cl-caspase-8 and RIP3 at 15 hpi showed similar distribution patterns. Altogether, these data revealed that each mutant virus induced a distinct pattern of caspase-8- and RIP3-dependent cell death signaling in BMDMs: an early RIP3 kinase-dependent, p-MLKL–mediated cascade driving necroptosis when caspase-8 is blocked and RHIM signal transduction is active; a later caspase-8/caspase-3–dependent signaling cascade triggering apoptosis when caspase-8 remains active and RHIM signaling is blocked; and a later caspase-8/caspase-3-dependent cascade triggering apoptosis that gives way to RIP3/pMLKL-dependent signaling events when both caspase-8 and RHIM signal transduction are active.

The combined signaling patterns observed in double-mutant virus-infected BMDMs led us to interrogate whether these events occurred in distinct subpopulations of cells. We optimized flow cytometric conditions to detect nonviable cells, using an amine-specific, fixable viability stain (FVS700), and assessed p-MLKL and cl-caspase-3 coexpression at 15 hpi (Fig. 2*B*). Some cross-reactivity of the p-MLKL Ab was observed with control *Mlkl*$^{-/-}$ BMDMs such that ∼3% of the ΔM36 and double-mutant virus-infected cells were identified as p-MLKL^{+}FVS700^{+} (Fig. 2*B*, *Upper*) cells expressing cl-caspase-3^{+} (Fig. 2*C*, *Upper*). This was not observed with uninfected or K181-bac or M45mutRHIM virus-infected cells. Whereas p-MLKL^{+}FVS700^{+} levels remained below 1% in uninfected and K181-bac virus-infected *Mlkl*$^{+/+}$ BMDM cultures (Fig. 2*B*, *Middle*), 9.8% of M45mutRHIM virus-infected cells were p-MLKL^{+}FVS700^{+}. Expectedly, these p-MLKL^{+}FVS700^{+} cells did not express cl-caspase-3 (Fig. 2*C*, *Bottom*). Relative to *Mlkl*$^{-/-}$ BMDMs, a nominal increase in p-MLKL^{+}FVS700^{+} levels (4.6%) was observed in ΔM36 virus-infected *Mlkl*$^{+/+}$ BMDMs. Remarkably, 11.1% of double-mutant virus-infected *Mlkl*$^{+/+}$ BMDM were p-MLKL^{+}FVS700^{+} and coexpressed cl-caspase-3. Furthermore, the profile emerging from the FVS700 vs. cl-caspase-3 plots distinguished ΔM36 from double-mutant virus-induced cell death as yielding more cl-caspase-3^{+} or p-MLKL^{+} cells, respectively (Fig. 2*B*, *Bottom*). Notwithstanding the modest Ab cross-reactivity, the increased frequency of p-MLKL^{+}cl-caspase-3^{+} BMDMs evident in double-mutant virus-infected cultures provides evidence of both caspase-8 and RIP3 signaling arms being triggered in the same cell.

An ATP release assay was used to compare changes in cell viability over time of infection with each of the four viruses (Fig. 2*D*). Even though caspase-8 and RIP3 activation were evident at 6–9 hpi with mutant viruses (Fig. 2*A*), 100% viability was observed in all BMDM cultures through 12 hpi (Fig. 2*D*). Viability only dropped slightly (15%) in K181-bac virus-infected cultures through 24 hpi, whereas a comparably sharp decline in viability (50–65%) was observed by 15 hpi with all three mutant viruses. Thus, by this assay, the time course of cell death appeared to be similar regardless of whether cell death suppressors were expressed and whether caspase-8 and/or RIP3 activation were triggered during infection.

Uptake of a cell permeant nucleic acid stain was combined with transmission electron microscopy to differentiate alterations in cell morphology associated with dying virus-infected BMDMs. K181-bac virus-infected BMDMs remained impermeable, as expected (Fig. 2*E*). The timing of M45mutRHIM virus-infected permeability coincided with the appearance of p-MLKL in these cells (Fig. 2*A*). Cell permeability developed after 12 hpi in both ΔM36 and double-mutant virus-infected cells (Fig. 2*E*) when modified insoluble RIP3 and p-MLKL were evident in double-mutant but not ΔM36 virus-infected BMDM cells (Fig. 2*A*). Thus, the appearance of cl-caspase-3 in ΔM36 and double-mutant virus-infected cells is concurrent with loss of cell viability and increased membrane permeability, whereas M45mutRHIM virus-infected cells remained viable long after p-MLKL and membrane permeability were evident. Transmission electron microscopic images of cells at 12 and 18 hpi revealed morphological changes consistent with cell leakage (Fig. 2*F*). Unlike uninfected cells that maintained a relatively smooth plasma membrane and elongated morphology (Fig. 2*F*), K181-bac virus-infected cells became rounded and enlarged with multiple vesicle-like structures by 12–18 hpi (Fig. 2*F*). ΔM36 virus-infected cells displayed the characteristic condensed chromatin in the nucleus and ruffled/blebbed plasma membrane of apoptosis by 12 hpi (Fig. 2*F*). In contrast, M45mutRHIM virus-infected cells contained large vacuoles by 12 hpi (Fig. 2*F*). Double-mutant virus-infected cells displayed a wider range of morphologies and, in some instances, simultaneously exhibited apoptotic (condensed chromatin and membrane ruffling/blebbing) and necroptotic features (vacuolated or lysed) within the same cell (Fig. 2*F*). Further, microscopy images capture classic blebbing/shrinkage during ΔM36 virus infection, cell lysis during M45mutRHIM virus infection, and flattened morphology before cell lysis in double-mutant virus-infected cells (Fig. S2*A* and Movies S1–S5). In *Mlkl*$^{-/-}$ BMDMs, M45mutRHIM virus did not induce death as expected, and the morphologies of cells dying from either the ΔM36 or double-mutant virus were indistinguishable (Fig. S2*B*). Altogether, these data demonstrate that RIP3 can subsequently function to activate MLKL and trigger secondary necroptosis even when caspase-8 is activated to drive apoptosis within individual virus-infected BMDMs.

Apoptosis with Secondary Necroptosis Occurs Independent of TNF and DAI That Sensitize BMDM to Respective ΔM36 or M45mutRHIM Virus-Induced Death. To understand the interplay between caspase-8 inhibition and RIP3 activities in the infected host, mice were inoculated i.p., using either of the four viruses, and replication in tissues was assessed. First, we set out to understand whether the early TNF-driven, caspase-8–dependent signaling during ΔM36 virus infection (22) and DAI-driven, RIP3-dependent signaling during M45mutRHIM virus infection (8) contribute to double-mutant virus-driven death. All three mutant viruses were attenuated in WT mouse spleens compared with K181 virus at 3 dpi (Fig. 3*A*), the peak time of replication in this organ. Activation of caspase-8 when RIP3 was inhibited triggered antiviral control in ΔM36 virus-infected spleens,

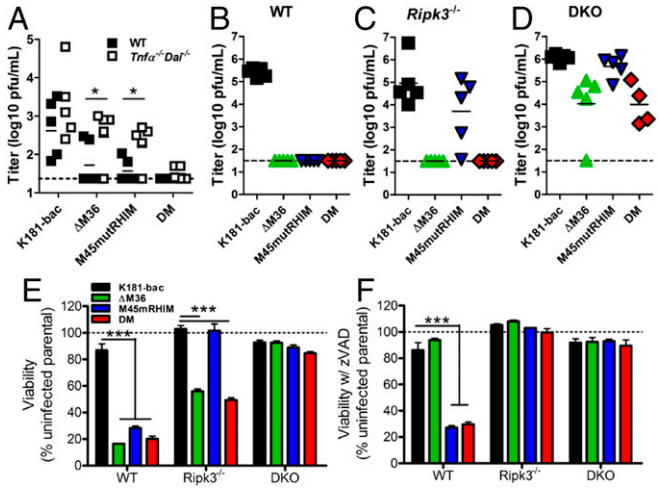

Fig. 3. MCMV M36 and M45 cooperate to suppress TNF/DAI-independent, caspase-8/RIP3-dependent cell death. (*A*) Replication of viruses in spleens of WT and $Tnf\alpha^{-/-}Dai^{-/-}$ mice inoculated i.p. with 10^6 plaque-forming units (PFU) virus and assessed at 3 dpi by plaque assay. (*B–D*) Viral titers in salivary glands at 14 dpi of (*B*) $Casp8^{+/+}$ $Ripk3^{+/+}$ (WT), (*C*) $Casp8^{+/-}Ripk3^{-/-}$ ($Ripk3^{-/-}$), and (*D*) DKO mice. Dashed horizontal lines depict the limit of detection of the assays. Horizontal dashed line indicates the limit of detection of the assay. (*E* and *F*) Viability of BMDM from WT, $Ripk3^{-/-}$, and DKO mice infected 18 h with either of the four viruses (MOI = 10) (*E*) without or (*F*) with zVAD. Horizontal dotted lines indicate 100% viability. Error bars indicate SD of the mean. $*P < 0.05$; $***P < 0.001$.

whereas inhibition of caspase-8 unleashed RIP3-dependent antiviral control during M45mutRHIM virus infection (Fig. 3*A*), as expected (7). The execution of caspase-8 and RIP3 activities together efficiently attenuated replication of double-mutant virus in spleens at 3 dpi. Expectedly, replication of both the ΔM36 and M45mutRHIM viruses were normalized in the $Tnf\alpha^{-/-}Dai^{-/-}$ spleens; however, double-mutant virus remained attenuated (Fig. 3*A*), suggesting that the combined TNF and DAI deficiency was not sufficient to overcome the M36-M45 defect during double-mutant virus infection. Thus, TNF- and DAI-independent sensors trigger the signaling cascade, limiting double-mutant virus infection in the host.

To directly query the consequences of caspase-8 signaling on RIP3 activity in infected host, viral titers in the salivary gland, an organ that best reflects successful infection of the host animal (28, 29), were assessed at 14 dpi of $Casp8^{+/+}Ripk3^{+/+}$ (WT), $Casp8^{+/-}Ripk3^{-/-}$ ($Ripk3^{-/-}$), and $Casp8^{-/-}Ripk3^{-/-}$ (DKO) littermate mice (Fig. 3 *B–D*). K181-bac virus disseminated to and replicated in salivary gland at this point, regardless of the mouse genotype. In contrast, ΔM36 virus was not detected in the salivary gland of WT mice (Fig. 3*B*), even though virus was detected in spleen (2/5) and liver (5/5) at 3 dpi (Fig. 3*A* and Fig. S3), consistent with previous reports (23). ΔM36 virus infection was normalized in DKO mice (Fig. 3*D*), but remained attenuated in $Ripk3^{-/-}$ mice (Fig. 3*C*). The attenuation of M45mutRHIM virus observed in WT mice (Fig. 3*B*) that is normalized in $Ripk3^{-/-}$ mice (Fig. 3*C*) (8) was also normalized in DKO mice (Fig. 3*B*). As expected from the pattern of death and poor replication in cultured cells, double-mutant virus was the most severely attenuated mutant in WT mice. Replicating virus was not detected in any tissue assessed (Fig. 3 *A* and *B* and Fig. S3). Replication of double-mutant virus was not normalized in $Ripk3^{-/-}$ mice (Fig. 3*C*), most likely because of unleashed caspase-8–dependent apoptosis in the absence of M36 (Fig. 1*M*), given that this virus was normalized in DKO cells and mice (Fig. 3*D*) and rescued by treatment with combined caspase and RIP3 inhibitor (Fig. 1*N*).

Consistent with mouse infection data, BMDMs infected with K181-bac virus remained viable regardless of host genotype (Fig. 3 *E* and *F*). Caspase-8 deficiency in DKO cells (Fig. 3*E*) or the addition of caspase inhibitor to WT and $Ripk3^{-/-}$ cultures (Fig. 3*F*) rescued cells from ΔM36 virus-induced death. RIP3 deficiency was sufficient to rescue cells from M45mutRHIM virus (Fig. 3*E*). Importantly, combined deficiency in caspase-8 and RIP3 restored viability of double-mutant-infected DKO (Fig. 3*E*). Caspase inhibition by zVAD rescued this virus in $Ripk3^{-/-}$ cells (Fig. 3*F*), but not in WT cells (Figs. 1*L* and 3*E*). Furthermore, $Mlkl^{-/-}$ BMDMs remained susceptible to double-mutant virus-induced death (Fig. S4 *A* and *B*), confirming apoptosis as the primary mode of death and the activation of RIP3/p-MLKL downstream of caspase-8 activation within the same population of cells. Altogether, these data confirm that RIP3-dependent cell death signaling occurs independent of caspase-8 inhibition in the MCMV-infected host and pinpoint the macrophage as a cell type that provides a correlate in behavior to the infected host.

A Distinctive FADD-Associated Ripoptosome-Like Complex Drives Apoptosis with Secondary Necroptosis. To better understand signaling events that sensitize BMDMs to double-mutant virus-induced death, we evaluated assembly of FADD-associated cytosolic molecular complexes at 12 hpi, a point at which cell death signaling is underway but cells are 100% viable. In uninfected BMDMs, immunoprecipitation of FADD showed spontaneous formation of a complex containing constitutively expressed FADD, RIP1, caspase-8, cFLIP, RIP3, and MLKL (Fig. 4*A*). K181-bac virus infection significantly reduced FADD, RIP3, and MLKL levels in this complex while modestly precluding caspase-8, despite abundance of these proteins in the cells (Fig. 4*A*). In contrast, ΔM36 virus infection drove greater FADD and caspase-8 recruitment into the complex, whereas RIP1 and cFLIP were precluded, concomitant with them being cleaved and/or declining in levels in the cytoplasm at 12 hpi (Fig. 4*A*). The complex was disrupted during M45mutRHIM virus infection such that FADD, RIP1, RIP3, and MLKL recruitment was not observed, concurrent with their partitioning into insoluble cell fractions (Fig. 4*A*). Remarkably, double-mutant virus infection promoted substantial recruitment of FADD, as well as the appearance of caspase-8 p43 and cFLIP p46 fragments within the complex (Fig. 4*A*). Thus, in accord with the TNF and DAI independence in sensitizing BMDMs, double-mutant virus drives the formation of a distinctive RIP1-containing complex (32, 33) that forms independent TNF signaling or DAI sensing and engages both caspase-8 and RIP3 signaling arms to trigger apoptosis with secondary necroptosis.

RIP1 regulates apoptotic and necroptotic cell death (32). Targeting of RIP1 to the Ripoptosome complex can be blocked by cIAP ubiquitylation. A role for cIAPs was not evident in infected WT BMDMs, given that treatment with increasing concentrations of the inhibitory drug, BV6, did not reverse the death induced by any of the mutant viruses (Fig. S4*C*). We next infected WT, $Ripk1^{K45A/K45A}$ (RIP1 kinase-dead; R1KD), and $Ripk1^{-/-}Casp8^{-/-}Ripk3^{+/-}$ (KKH) BMDMs with any of the four viruses (Fig. 4 *B–E*). RIP1 kinase activity was dispensable for cell death induced by mutant viruses, given that gene disruption did not rescue cells from death (Fig. 4 *B*, *D*, and *E*), although gene disruption (Fig. 4*D*) and necrostatin-1 inhibition (Fig. S4*D*) of RIP1 kinase activity did influence the timing of M45mutRHIM virus-induced necroptosis [i.e., after 6 hpi in WT cells (Fig. 4*C*) vs. after 12 hpi in R1KD cells (Fig. 4*D*)]. Caspase-8 deficiency in KKH mice rescued BMDMs from ΔM36 virus-induced, but not double-mutant virus-induced, death (Fig. 4*E*). Here, caspase-8 deficiency directed double-mutant virus to behave like the M45mutRHIM virus in these cells, causing an even more delayed pattern of necroptosis (after 18 hpi), likely because of the combined loss of RIP1 activity and one allele of RIP3 (Fig. 4 *B–E*). Thus, a picture emerges from MCMV-infected BMDMs in which, on one hand, caspase-8 inhibition is likely to facilitate RIP1 kinase activity-dependent licensing of early necroptosis without

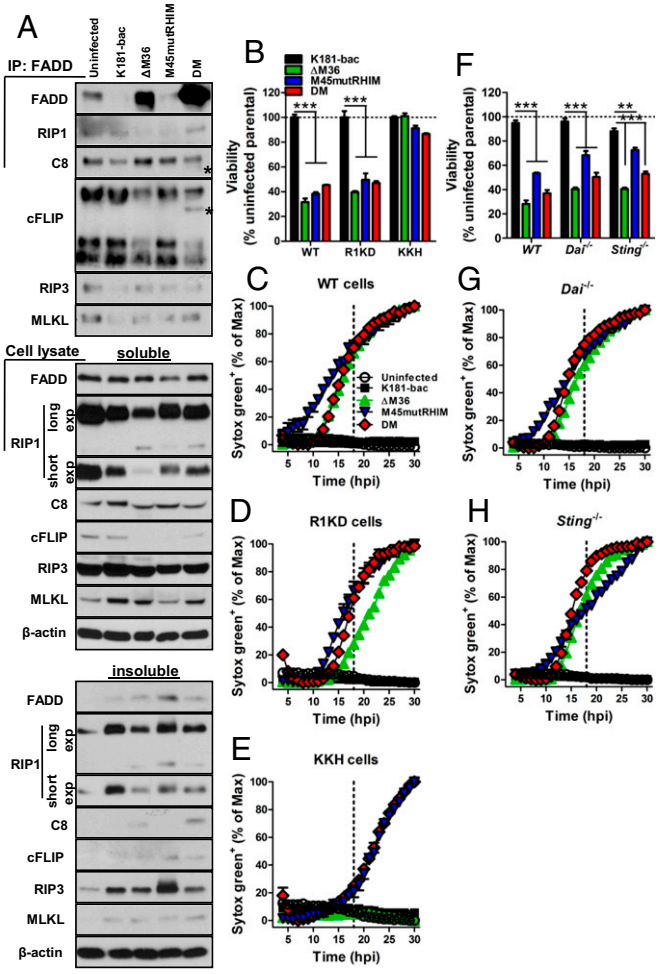

Fig. 4. Distinct FADD-associated complex drives apoptosis with secondary necroptosis. (*A*) Molecular complex association in uninfected and MCMV-infected BMDMs. Cells were lysed at 12 hpi and lysate incubated with FADD Abs, and associated proteins were detected by immunoblot. Triton X soluble and insoluble cell lysate fractions were examined in parallel. Asterisks denote cleavage products. (*B–E*) Viability at 18 hpi (*B*) and STYOX Green uptake in BMDMs from (*C*) WT, (*D*) *Ripk1*$^{K45A/K45A}$ (R1KD), and (*E*) KKH mice. (*F–H*) Viability at 18 (*F*) and STYOX Green uptake in BMDMs from (*G*) *Dai*$^{-/-}$ or (*H*) *Sting*$^{-/-}$ mice. Error bars indicate SD of the mean. Dashed vertical lines depict 18 hpi when viability assays were conducted. Horizontal dotted lines indicate 100% viability. $^{**}P < 0.01$; $^{***}P < 0.001$.

apoptosis and, on the other hand, when caspase-8 function is unrestricted, a Ripoptosome-like machinery triggers apoptosis followed by necroptosis.

We next sought to compare the contribution of DAI with the known virus sensor, stimulator of IFN genes (STING), in infected BMDMs. A modest increase in cell viability was observed in all mutant virus-infected *Dai*$^{-/-}$ compared with WT cells at 18 hpi (Fig. 4*F*), with no effect on the inevitable cell death (Fig. 4*G*). Even though DAI deficiency rescues the M45mutRHIM defect in MEFs and at the site of entry in mice (8), this sensor is dispensable in BMDMs consistent with the partial rescue of the myeloid cell-dependent dissemination of virus to the salivary gland of infected *Dai*$^{-/-}$ mice (8). Similarly, STING deficiency only partially rescued viability with no effect on death of mutant virus-infected BMDMs (Fig. 4 *F* and *H*). Overall, known DNA sensors involved in early signaling events to virus infections were dispensable to double-mutant virus-induced death.

TLR sensing in BMDM appears dispensable to cell death signaling cascades triggered in response to ΔM36, M45mutRHIM, and double-mutant virus infection, given that cells from *MyD88*$^{-/-}$ and *Ticam1*^{Lps2} (Trif$^{-/-}$) mice remained sensitive to apoptotic and necroptotic cell death (Fig. S4 *E–G*). Combined, these data demonstrate that double-mutant virus infection drives the assembly of a FADD-RIP1-caspase-8(p43)-cFLIP(p46)-RIP3-MLKL complex independent of DAI, STING, or TLR sensing to mediate apoptosis with secondary necroptosis in BMDMs when both caspase-8 and RIP3 activation are engaged. This is consistent with the Ripoptosome itself likely acting as a pathogen sensor, as hypothesized (19, 27).

Double-Mutant Virus-Induced Combined Apoptosis with Necroptosis Is Proinflammatory and Generates Robust Innate Responses in the Host. Although both apoptotic and necroptotic forms of cell death may be proinflammatory in the proper context, their relative contribution to inflammation and inflammatory disease remain unresolved. Assessment of BMDM culture supernatants revealed disparate proinflammatory cytokine production after infection with either of the four viruses through 18 h (Fig. 5*A*). K181-bac virus stimulated modest production of IL-6, TNF, and IL-1β with high levels of KC (murine IL-8) and IL-10 (Fig. 5*A*). Whereas ΔM36 virus infection amplified TNF production, consistent with TNF-driven death (22), while dampening IL-10 levels, M45mutRHIM virus also did not produce much IL-10, yet IL-6, TNF, and IL-1β production did not surpass K181-bac virus levels. Remarkably, double-mutant virus-infected WT BMDMs produced significant quantities of IL-6 with TNF, even though IL-10 production was elevated. No infection settings induced IFN-γ, IL-12p70, IL-2, IL-4, or IL-5 production during this time. *Rip3k*$^{-/-}$ cells were assessed to interrogate the consequence of RIP3 signaling on cytokine production. RIP3 deficiency had disparate consequences on cytokine production (Fig. 5*B*). A general decline in TNF, KC, and IL-10 levels was observed, whereas IL-1β production increased after ΔM36 and double-mutant virus infection. Even though IL-6 production declined in all but ΔM36 virus-infected *Rip3*$^{-/-}$ BMDM cultures, levels induced by double-mutant virus were equivalent to that of ΔM36 virus. These data suggest dispensability of RIP3 function in IL-6 cytokine production during apoptosis but strongly implicate RIP3 activation that signals secondary necroptosis during double-mutant virus infection as a determinant of proinflammatory death.

To determine whether the cell death processes modulate antiviral innate responses, we infected C57BL/6 mice with K181-bac or one of the cell death-inducing mutants and quantified cytokine responses in the spleen. For these in vivo investigations, we chose 18 hpi, given that equivalent levels of cell death were observed in mutant virus-infected BMDM at this point in vitro (Fig. 1*L*). Compared with uninfected spleens, a similar increase in frequencies of dead cell events was evident in K181-bac and ΔM36 virus-infected spleens; however, frequencies were significantly increased in M45mutRHIM and double-mutant virus-infected spleens (Fig. 5*C*). In addition, splenic macrophage numbers decreased fourfold during M45mutRHIM and double-mutant virus infections, whereas numbers in K181-bac and ΔM36 spleens remained equivalent to uninfected mice (Fig. 5*D*). K181-bac virus recruited inflammatory monocytes (Fig. 5*E*), but not neutrophils (Fig. 5*F*), at this point. Whereas inflammatory infiltrates had not been recruited to ΔM36 virus-infected spleens (Fig. 5 *E* and *F*), neutrophils had started to accumulate in M45mutRHIM virus-infected spleens (Fig. 6*D*). In contrast, significant numbers of both inflammatory monocytes (Fig. 5*E*) and neutrophils (Fig. 5*F*) were recruited to double-mutant virus-infected spleens. Thus, the double-mutant virus displayed a remarkably distinct ability to stimulate inflammatory infiltration in infected mice.

Evaluation of proinflammatory cytokines produced during infection showed that K181-bac and M45mutRHIM viruses induced IL-12p70, IFN-γ, IL-6, TNF-α, IL-2, and KC production to similar levels in the host by 18 hpi; however, K181-bac virus

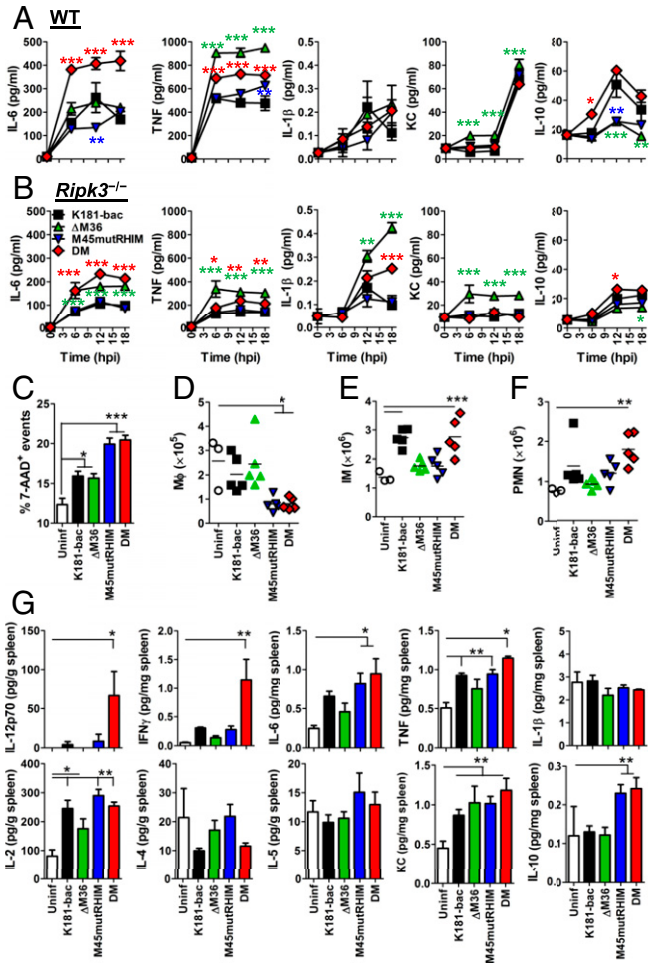

Fig. 5. Assessment of caspase-8 and RIP3 activation on cell death and innate inflammatory response. (*A* and *B*) Cytokine production in (*A*) WT and (*B*) *Ripk3*$^{-/-}$BMDM cultures after infection with either of the four viruses. Infections were performed in triplicate wells, culture supernatant was collected at specified times, and cytokine levels were quantified by ELISA. Colored asterisks denote significance differences of respectively colored symbols relative to K181-bac virus infection. (*C*) Frequency of dead cell events in spleens of WT mice infected with any of the four viruses. (*D*–*F*) Total numbers of splenic (*D*) macrophages (MΦ), (*E*) inflammatory monocytes (IM) and (*F*) neutrophils (PMN). (*G*) Cytokine concentration in spleens. Spleens were collected from infected mice at 18 hpi and homogenized for cytokine quantification by ELISA. Error bars represent SE of the mean. **P* < 0.05; ***P* < 0.01; ****P* < 0.001.

dampened IL-4 expression, whereas ΔM36 virus stimulated IL-10 production (Fig. 5*G*). Most important, however, were the distinctions between the cytokine patterns induced by the two proapoptotic viruses. ΔM36 virus-triggered, caspase-8–mediated extrinsic apoptosis induced an overall dampened cytokine response compared with K181-bac virus; however, double-mutant virus-triggered apoptosis with secondary necroptosis was the most proinflammatory infection setting. The inflammatory cues defining double-mutant virus infection in the host were marked by a >10-fold increase in IL-12p70 and IFN-γ production, as well as elevated IL-6 and TNF production compared with K181-bac infection, even though IL-10 production was evident. Although infected macrophages are a source of IL-6, TNF, and IL-10 (Fig. 5*A*), expectedly, both DCs and macrophages produce IL-12p70, whereas Ly49H^{+} NK cells produce IFN-γ at this time (Fig. S5). IL-2 and KC production, as well as the down-regulation of IL-4 expression were comparable to K181-bac virus infection. In aggregate, caspase-8 together with RIP3 activation signals a proinflammatory cell death cascade in MCMV-infected macrophages and stimulates robust proinflammatory cytokine responses in the infected host.

Proinflammatory Apoptosis with Secondary Necroptosis Elicits Early CD8 T-cell Responses. To assess the immunologic consequence of apoptotic and necroptotic cell death on adaptive immunity, CD8 T-cell responses were evaluated in spleens of C57BL/6 mice infected with the four viruses (Fig. 6). Replication-competent K181-bac and ΔM36 viruses were detected at 7 dpi in spleens of infected mice, whereas neither of the replication-deficient M45mutRHIM nor double-mutant viruses were detected at this time (Fig. 6*A*). Whereas peak CD8 T-cell proliferative and differentiation responses were observed at 7 dpi during K181-bac and single-mutant (albeit to a lesser extent) virus infections, remarkably, the response to double-mutant virus infection was faster, initiating at 3 dpi to peak by 5 dpi (Fig. 6 *B*–*D*). K181-bac and ΔM36 virus-induced CD8 T cells exhibited the phenotype of short-lived effector cells (KLRG1^{+}CD127^{-}) at this time (Fig. 6 *E* and *F*). M45mutRHIM virus-induced cells displayed a mixed pattern, peaking at 7 dpi with equivalent numbers of short-lived effector cells and memory precursor effector cells (KLRG1^{-}CD127^{+}).

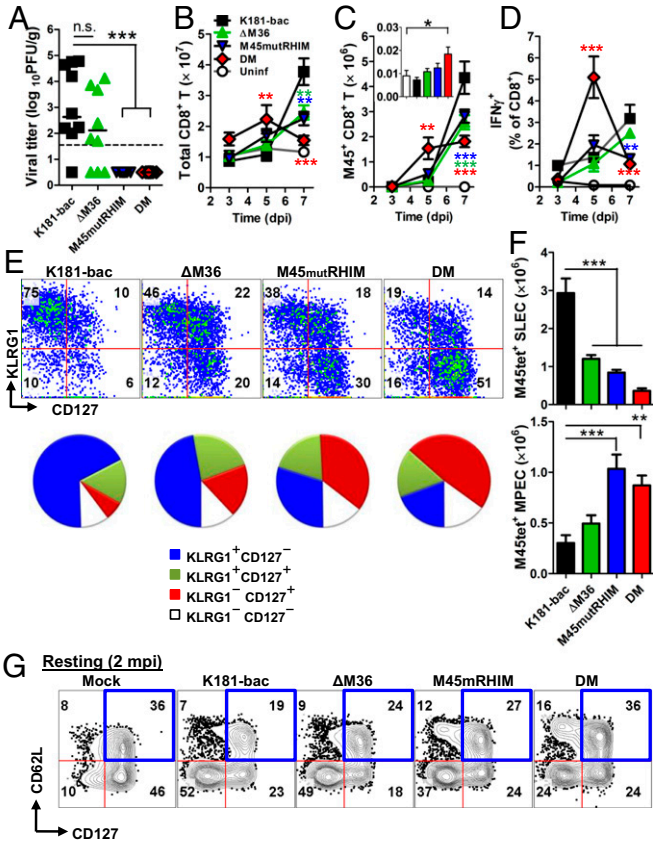

Fig. 6. In vivo assessment of caspase-8 and RIP3-mediated cell death on cell death antiviral CD8 T-cell responses. (*A*) Viral titers at 7 dpi in spleens of infected WT mice Horizontal lines represent mean. (*B*–*D*) Total (*B*), M45 tetramer-positive (*C*), (inlay; 3 dpi), and IFN-γ^{+} M45 peptide-simulated (*D*) CD8 T cells in spleens. (*E*) Flow cytometry plots and pie charts showing KLRG1 and CD127 expression and (*F*) total numbers of short-lived effector cell (KLRG1^{+}CD127^{-}) and memory precursor effector cell (KLRG1^{-}CD127^{+}) M45 tetramer positive CD8 T cells at 7 dpi. (*G*) Flow cytometry plots showing CD62L and CD127 expression on Ag-experienced CD11a^{+}CD49d^{+} CD8 T cells in spleens at 60 dpi. Spleens were collected from infected mice at specified time points. Error bars represent SD of the mean. **P* < 0.05; ***P* < 0.01; ****P* < 0.001.

By this time, double-mutant virus-induced T cells had already started to contract with a predominance of memory precursor effector cells. Thus, the proinflammatory nature of double-mutant virus-induced death elicited faster primary CD8 T-cell responses and memory pool development in the infected host.

To interrogate the robustness of adaptive immunity generated during primary infection, mice were rested 60 d and then challenged with a *lac*Z-expressing K181 mutant to compared protection. At this point, double-mutant virus infection had maintained twice the frequency of memory CD8 T cells displaying markers consistent with a highly protective $CD62L^{+}CD127^{+}$ phenotype (Fig. 6*G*). On challenge, no mice became superinfected, as evidenced by the lack of detectable replicating virus (no blue or white plaques in plaque assays) in any tissues assessed. Thus, inflammation and immunogenicity associated with double-mutant virus-infected cells that precipitated antiviral CD8 T-cell responses during primary infection generated protective anamnestic responses in the host.

Discussion

This work validates the role of regulated cell death pathways in host defense. Somewhat surprisingly, caspase-8 suppression of the necroptotic trapdoor is not as prevalent in a natural mouse virus infection. Although suggested based on studies involving a poxvirus (12), HSV-infected human carcinoma cells (26), as well as mouse embryogenesis (9), caspase-8 suppression of the RIP3/MLKL machinery does not play out either in virus-infected BMDMs or during natural infection in the host. Here, we investigate the effect of caspase-8 activity on triggering RIP3-dependent necroptosis during MCMV infection, relying on individual or combined M36 and M45 mutant phenotypes. In BMDMs, necroptosis is triggered whether or not caspase-8 is inhibited or activated during infection. When M36 inhibits caspase-8 function, RIP3 signals necroptosis early. In contrast, when caspase-8 is activated to initiate apoptosis, necroptosis is nonetheless the outcome, albeit with delayed kinetics. Apoptosis with secondary necroptosis is highly proinflammatory in the host, compared with other infection settings, suggesting M36 and M45 collaborate to suppress antiviral and, importantly, proinflammatory consequences of cell death signaling.

Patrolling monocyte-derived cells such as macrophages are important in MCMV dissemination (28, 34) and are crucial players in HCMV pathogenesis that are targeted by virus-encoded inhibitors of caspase-8– and mitochondrial-dependent apoptosis (35). It seems fitting, therefore, that MCMV infection sensitizes BMDMs to both apoptosis and necroptosis, without the cross-regulation that is observed in endothelial and other cell types, as these are the cells within which the importance of combined M36 and M45 functions play out. The remarkable parallels between infection outcome in macrophages and the host bolster the physiological importance of M36 and M45 synergism in subverting cell death in macrophages. This synergy prevents elimination of virus-infected cells crucial for dissemination while also reducing the inflammatory consequences of a systemic viral infection, preserving crucial properties that define dissemination and persistence. HCMV also encodes an inhibitor of caspase-8 activation (UL36) (17) and blocks RIP3-dependent necroptosis, although downstream of MLKL (36). Consistently, the MCMV model has reliably predicted principles of pathogen–host interactions at play during HCMV infection. The similarities between the MCMV- and HCMV-encoded cell death suppressor functions likely predicts a similar caspase-8 and RIP3-driven cell death signaling cascade that is triggered in human myeloid/macrophage cells.

Double-mutant MCMV drives a pattern of regulated death that does not appear to depend on any sensor other than the Ripoptosome components themselves. This pattern aligns with the role of these cytosolic components as a "pathogen supersensor" to detect infection or other cellular insult. Given that the combined apoptotic–necroptotic pathway is independent of both TNF signaling and DAI sensing, the pattern we have characterized is completely distinct from either single mutant: ΔM36 and M45mutRHIM. Thus, caspase-8 and RIP3 have the ability to drive a collaborative death signaling cascade when both viral M36 and M45 inhibitors are absent. TNF synergizes with IFN-γ to effect antiviral activity (37) through the engagement of FADD-dependent death receptors that would propagate caspase-8–dependent apoptotic signaling had it not been for M36 inhibition of caspase-8 activation (22, 23, 38). Similarly, DAI RHIM-meditated interactions in infected cells initiates a RHIM-dependent RIP3-mediated signaling cascade that would induce necroptosis if not for M45 RHIM-dependent disruption of signal transduction (7, 8, 25, 39). Regardless of whether the Ripoptosome components themselves act as a sensor, the data here do not inculpate any TLRs, whether MyD88- or TRIF-dependent, upstream of cell death signaling induced by a virus that fails to block caspase-8 activation as well as RHIM signal transduction.

The evidence presented in this manuscript represents a report of a virus infection triggering apoptosis with secondary necroptosis where RIP3 activation governs the extent of the proinflammatory consequences. The extent to which the combined signaling process contributes to driving inflammation in response to dying, infected cells is not fully understood. The dual cell death signaling elicited by double-mutant virus is remarkably proinflammatory compared with either ΔM36 or M45mutRHIM viruses, or to even the gold standard response to K181-bac virus infection. Notably, neither apoptosis nor necroptosis occurring in the infected host was proinflammatory, as both processes elicit comparably dampened cytokine responses independent of virus replication competence. Given the proinflammatory nature of the dual cell death unleashed during double-mutant virus infection, one can perceive how this process likely effected evolution of M36- and M45-encoded inhibitory functions to not only suppress cell death in the infected cell but also delay the proinflammatory alarm response in neighboring and innate cells. Together, these functions are equally important to viral persistence in the infected host.

Altogether, we have shown that caspase-8 inhibition is not necessary to trigger virus-induced, RIP3-mediated necroptosis as this process proceeds regardless of caspase-8 activation. Our data did reveal, however, that caspase-8 inhibition permitted RIP1 kinase-dependent precipitation of the necroptotic process. In the absence of both M36 and M45 suppressors, MCMV infection triggers caspase-8 activation before unleashing delayed RIP3-mediated cell death signal transduction in infected BMDM, resulting in dual apoptotic–necroptotic cell death. We now understand that simultaneous engagement of caspase-8 and RIP3 cell death signaling in the host cell has highly proinflammatory consequences.

Materials and Methods

Mice and Experimental Infection. C57BL/6J mice (Jackson Laboratory), *Ripk3*$^{-/-}$, DKO (9), KKH (40), *Ripk1*$^{K45A/K45A}$ (41), and *TNFα*$^{-/-}$*Dai*$^{-/-}$ generated by crossing *Dai*$^{-/-}$ mice (42) with *Tnfα*$^{-/-}$ mice (B6;129S-*Tnf*^{tm1Gkl}/J; Jackson Laboratory) were used in this study. Inoculations were via the i.p. route with 10^6 PFU virus in DMEM or medium only (mock). Mice were housed at the Emory University Division of Animal Resources, where experiments were conducted according to National Institutes of Health and Emory University Institutional Animal Care and Use Committee guidelines.

Viruses, Cells, and Infection. Viruses used in this study [K181-bac and M45*mut*RHIM (6) and ΔM36 and ΔM36/M45*mut*RHIM (described in *SI Materials and Methods*) (6, 7, 43–45)] were propagated on NIH 3T3s and quantified by plaque assay (46). Cells used were NIH 3T3, SVEC4-10, MEFs, and BMDMs generated from C57BL/6J, *Ripk3*$^{-/-}$, DKO, *Ripk1*$^{K45A/K45A}$, KKH, *Mlkl*$^{-/-}$, and *Mlkl*$^{+/+}$, *Sting*$^{-/-}$ (Dr. Li, UTSA) or *Ticam*^{lps} and *Myd88*$^{-/-}$ (Bali Pulendran) mice. Infections were carried out by incubating cells with virus for 1 h (MOI = 5 or MOI = 10 for BMDM), at which time inocula were replaced with fresh medium and then incubated for specified times. For plaque assays, homogenized

tissues or culture supernatant were overlaid onto NIH 3T3 monolayers and plaques enumerated from fixed, Giemsa-stained cells (29).

Immunoprecipitation and Immunoblots. Whole-cell extracts were prepared using lysis buffer [50 mM Tris, 150 mM NaCl, 5 mM EDTA, 1% Triton X-100, and phosphatase and protease inhibitors (Roche; 1 tablet/10 mL each)], and clarified cell lysates were incubated overnight with anti-FADD, and then for 2 h with protein A/G agarose (Santa Cruz). For immunoblots, samples were resolved in 4–20% Midi Protean TGX gels (Bio-Rad); proteins were transferred to Immobilon PVDF membrane (Millipore) and developed using specified Abs.

Cell Viability. Cells were incubated 18 h, and then viability was assessed using Cell Titer-Glo Luminescent Cell Viability Assay (Promega) (7). Values depict viability as a percentage of uninfected or K181-bac virus-infected cells. Alternatively, infected cells were cultured with 62.5 nM SYTOX Green (Invitrogen), a live-cell impermeant nucleic acid fluorescent dye, and analyzed by an IncuCyte ZOOM live-cell imaging and analysis system (Essen Biosystems). Green cells per square millimeter were calculated from four images at indicated points.

Flow Cytometry. BMDMs were infected 15 hpi, and nonviable cells were tagged with amine-specific FVS700 (yields variable staining with apoptotic cells, as per manufacturer's notes) before staining for signaling molecules p-MLKL and cl-caspase-3. For immune response analyses, spleens were harvested from mice at 18 hpi and processed as described (29). Data were acquired using a BD LSRII cytometer equipped with five lasers and FACSDiva Software (BD Biosciences), analyzed with FlowJo (TreeStar), and graphed with Prism (GraphPad).

Statistical Analysis. Student's *t* test or one-way ANOVA or two-way ANOVA with Bonferroni's or Dunnett's Multiple Comparison posttest analyses were conducted using GraphPad Prism 5. $P \leq 0.05$ was considered significant.

Additional methods are detailed in the *SI Materials and Methods*.

ACKNOWLEDGMENTS. We thank Kerrie Yeung for technical assistance, Rafi Ahmed and Sam Speck for reagents, Jason Upton for technical advice, and Siddarth Balachandran and the E.S.M. laboratory members for comments on the manuscript. This work was supported by Public Health Service Grants R01 AI020211 and R01 AI118853 (to E.S.M.) and in part by the Flow Cytometry Core Facility of the Emory Vaccine Center.

1. Mocarski ES, Guo H, Kaiser WJ (2015) Necroptosis: The Trojan horse in cell autonomous antiviral host defense. *Virology* 479-480:160–166.
2. Sun X, et al. (1999) RIP3, a novel apoptosis-inducing kinase. *J Biol Chem* 274(24): 16871–16875.
3. Newton K, et al. (2014) Activity of protein kinase RIPK3 determines whether cells die by necroptosis or apoptosis. *Science* 343(6177):1357–1360.
4. Mandal P, et al. (2014) RIP3 induces apoptosis independent of pronecrotic kinase activity. *Mol Cell* 56(4):481–495.
5. Nogusa S, et al. (2016) RIPK3 activates parallel pathways of MLKL-driven necroptosis and FADD-mediated apoptosis to protect against influenza A virus. *Cell Host Microbe* 20(1):13–24.
6. Upton JW, Kaiser WJ, Mocarski ES (2008) Cytomegalovirus M45 cell death suppression requires receptor-interacting protein (RIP) homotypic interaction motif (RHIM)-dependent interaction with RIP1. *J Biol Chem* 283(25):16966–16970.
7. Upton JW, Kaiser WJ, Mocarski ES (2010) Virus inhibition of RIP3-dependent necrosis. *Cell Host Microbe* 7(4):302–313.
8. Upton JW, Kaiser WJ, Mocarski ES (2012) DAI/ZBP1/DLM-1 complexes with RIP3 to mediate virus-induced programmed necrosis that is targeted by murine cytomegalovirus vIRA. *Cell Host Microbe* 11(3):290–297.
9. Kaiser WJ, et al. (2011) RIP3 mediates the embryonic lethality of caspase-8-deficient mice. *Nature* 471(7338):368–372.
10. Oberst A, et al. (2011) Catalytic activity of the caspase-8-FLIP(L) complex inhibits RIPK3-dependent necrosis. *Nature* 471(7338):363–367.
11. Zhang H, et al. (2011) Functional complementation between FADD and RIP1 in embryos and lymphocytes. *Nature* 471(7338):373–376.
12. Cho YS, et al. (2009) Phosphorylation-driven assembly of the RIP1-RIP3 complex regulates programmed necrosis and virus-induced inflammation. *Cell* 137(6): 1112–1123.
13. Zhang DW, et al. (2009) RIP3, an energy metabolism regulator that switches TNF-induced cell death from apoptosis to necrosis. *Science* 325(5938):332–336.
14. He S, et al. (2009) Receptor interacting protein kinase-3 determines cellular necrotic response to TNF-alpha. *Cell* 137(6):1100–1111.
15. Kaiser WJ, et al. (2013) Toll-like receptor 3-mediated necrosis via TRIF, RIP3, and MLKL. *J Biol Chem* 288(43):31268–31279.
16. Guo H, Kaiser WJ, Mocarski ES (2015) Manipulation of apoptosis and necroptosis signaling by herpesviruses. *Med Microbiol Immunol (Berl)* 204(3):439–448.
17. Skaletskaya A, et al. (2001) A cytomegalovirus-encoded inhibitor of apoptosis that suppresses caspase-8 activation. *Proc Natl Acad Sci USA* 98(14):7829–7834.
18. Langelier Y, et al. (2002) The R1 subunit of herpes simplex virus ribonucleotide reductase protects cells against apoptosis at, or upstream of, caspase-8 activation. *J Gen Virol* 83(Pt 11):2779–2789.
19. Mocarski ES, Upton JW, Kaiser WJ (2011) Viral infection and the evolution of caspase 8-regulated apoptotic and necrotic death pathways. *Nat Rev Immunol* 12(2):79–88.
20. Rebsamen M, et al. (2009) DAI/ZBP1 recruits RIP1 and RIP3 through RIP homotypic interaction motifs to activate NF-kappaB. *EMBO Rep* 10(8):916–922.
21. Krause E, de Graaf M, Fliss PM, Dölken L, Brune W (2014) Murine cytomegalovirus virion-associated protein M45 mediates rapid NF-κB activation after infection. *J Virol* 88(17):9963–9975.
22. Ebermann L, et al. (2012) Block of death-receptor apoptosis protects mouse cytomegalovirus from macrophages and is a determinant of virulence in immunodeficient hosts. *PLoS Pathog* 8(12):e1003062.
23. Cicin-Sain L, et al. (2008) Dominant-negative FADD rescues the in vivo fitness of a cytomegalovirus lacking an antiapoptotic viral gene. *J Virol* 82(5):2056–2064.
24. Ménard C, et al. (2003) Role of murine cytomegalovirus US22 gene family members in replication in macrophages. *J Virol* 77(10):5557–5570.
25. Brune W, Ménard C, Heesemann J, Koszinowski UH (2001) A ribonucleotide reductase homolog of cytomegalovirus and endothelial cell tropism. *Science* 291(5502):303–305.
26. Guo H, et al. (2015) Herpes simplex virus suppresses necroptosis in human cells. *Cell Host Microbe* 17(2):243–251.
27. Mocarski ES, Kaiser WJ, Livingston-Rosanoff D, Upton JW, Daley-Bauer LP (2014) True grit: Programmed necrosis in antiviral host defense, inflammation, and immunogenicity. *J Immunol* 192(5):2019–2026.
28. Daley-Bauer LP, Roback LJ, Wynn GM, Mocarski ES (2014) Cytomegalovirus hijacks CX3CR1(hi) patrolling monocytes as immune-privileged vehicles for dissemination in mice. *Cell Host Microbe* 15(3):351–362.
29. Daley-Bauer LP, Wynn GM, Mocarski ES (2012) Cytomegalovirus impairs antiviral CD8+ T cell immunity by recruiting inflammatory monocytes. *Immunity* 37(1): 122–133.
30. Li J, et al. (2012) The RIP1/RIP3 necrosome forms a functional amyloid signaling complex required for programmed necrosis. *Cell* 150(2):339–350.
31. Moriwaki K, Chan FK (2016) Regulation of RIPK3- and RHIM-dependent necroptosis by the proteasome. *J Biol Chem* 291(11):5948–5959.
32. Feoktistova M, et al. (2011) cIAPs block Ripoptosome formation, a RIP1/caspase-8 containing intracellular cell death complex differentially regulated by cFLIP isoforms. *Mol Cell* 43(3):449–463.
33. Tenev T, et al. (2011) The Ripoptosome, a signaling platform that assembles in response to genotoxic stress and loss of IAPs. *Mol Cell* 43(3):432–448.
34. Daley-Bauer LP, Mocarski ES (2013) Myeloid cell recruitment and function in cytomegalovirus immunity and pathogenesis. *Cytomegaloviruses: From Molecular Pathogenesis to Intervention*, ed Reddehase MJ (Caister Scientific Press, Norfolk), Vol I, pp 363–373.
35. McCormick AL, Mocarski ES (2013) Cell death pathways controlled by cytomegaloviruses. *Cytomegaloviruses: From Molecular Pathogenesis to Intervention*, ed Reddehase MJ (Caister Scientific Press, Norfolk), Vol I, pp 263–276.
36. Omoto S, et al. (2015) Suppression of RIP3-dependent necroptosis by human cytomegalovirus. *J Biol Chem* 290(18):11635–11648.
37. Lucin P, et al. (1994) Late phase inhibition of murine cytomegalovirus replication by synergistic action of interferon-gamma and tumour necrosis factor. *J Gen Virol* 75(Pt 1):101–110.
38. McCormick AL, Skaletskaya A, Barry PA, Mocarski ES, Goldmacher VS (2003) Differential function and expression of the viral inhibitor of caspase 8-induced apoptosis (vICA) and the viral mitochondria-localized inhibitor of apoptosis (vMIA) cell death suppressors conserved in primate and rodent cytomegaloviruses. *Virology* 316(2): 221–233.
39. Mack C, Sickmann A, Lembo D, Brune W (2008) Inhibition of proinflammatory and innate immune signaling pathways by a cytomegalovirus RIP1-interacting protein. *Proc Natl Acad Sci USA* 105(8):3094–3099.
40. Kaiser WJ, et al. (2014) RIP1 suppresses innate immune necrotic as well as apoptotic cell death during mammalian parturition. *Proc Natl Acad Sci USA* 111(21):7753–7758.
41. Berger SB, et al. (2014) Cutting Edge: RIP1 kinase activity is dispensable for normal development but is a key regulator of inflammation in SHARPIN-deficient mice. *J Immunol* 192(12):5476–5480.
42. Ishii KJ, et al. (2008) TANK-binding kinase-1 delineates innate and adaptive immune responses to DNA vaccines. *Nature* 451(7179):725–729.
43. Redwood AJ, et al. (2005) Use of a murine cytomegalovirus K181-derived bacterial artificial chromosome as a vaccine vector for immunocontraception. *J Virol* 79(5): 2998–3008.
44. Tandon R, Mocarski ES (2008) Control of cytoplasmic maturation events by cytomegalovirus tegument protein pp150. *J Virol* 82(19):9433–9444.
45. Tischer BK, Smith GA, Osterrieder N (2010) En passant mutagenesis: A two step markerless red recombination system. *Methods Mol Biol* 634:421–430.
46. Saederup N, Lin YC, Dairaghi DJ, Schall TJ, Mocarski ES (1999) Cytomegalovirus-encoded beta chemokine promotes monocyte-associated viremia in the host. *Proc Natl Acad Sci USA* 96(19):10881–10886.